Coherent population trapping in diamond N-V centers at zero magnetic field

Coherent Population Trapping in Diamond N-V Centers at Zero Magnetic Field

Charles Santori[1],* David Fattal[1], Sean M. Spillane[1], Marco Fiorentino[1], Raymond G. Beausoleil[1], Andrew D. Greentree[2,4], Paolo Olivero[4], Martin Draganski[5], James R. Rabeau[4], Patrick Reichart[4], Brant C. Gibson[3,4], Sergey Rubanov[2,4], David N. Jamieson[2,4], and Steven Prawer[2,4]

[1] *Hewlett-Packard Laboratories, 1501 Page Mill Rd., Palo Alto, CA 94304*

[2] *Centre for Quantum Computer Technology*

[3] *Quantum Communications Victoria*

[4] *School of Physics, The University of Melbourne, Melbourne, Victoria 3010, Australia and*

[5] *Applied Physics, RMIT University, GPO Box 2476V, Melbourne, Victoria 3001, Australia*

(Dated: March 24, 2006)

Abstract

Coherent population trapping at zero magnetic field was observed for nitrogen-vacancy centers in diamond under optical excitation. This was measured as a drop in fluorescence when the detuning between two lasers matched the 2.88 GHz crystal-field splitting of the ground states. The behavior is highly sensitive to strain, which modifies the excited states. The results demonstrate that three-level Lambda configurations suitable for proposed quantum information applications can be realized simultaneously for all four orientations of nitrogen-vacancy centers at zero magnetic field.

PACS numbers: 42.50.Gy, 42.62.Fi, 78.67.-n

Impurity spins in solids are appealing as physical systems for quantum information processing, combining long decoherence times with the possibility for large-scale integration based on semiconductor processing technology [1]. Of the various impurities offering access to individual electron spins, one of the most promising is the nitrogen-vacancy (N-V) center in diamond, which consists of a substitutional nitrogen atom next to a carbon vacancy. Electron spin coherence times up to $58\,\mu$s have been measured at room temperature [2], and optical readout of the electronic spin state of a single negatively-charged N-V center (NV^-) has been demonstrated [3]. Controlled coupling between electonic and nuclear spins has been demonstrated [4, 5], offering potentially much longer storage times, and controlled coupling with nearby nitrogen impurities is also possible [6]. Single-photon generation at room temperature [7, 8] has demonstrated the utility of N-V centers for quantum communication. Based on such experimental results, schemes for quantum memories and repeaters [9] and quantum computation using electron spins [10–12] have been proposed.

Most experiments to date have relied on microwave fields to manipulate the electron spins and have used optical fields mainly for readout. All-optical control would allow for spatially selective addressing of single or a few N-V centers [12] and could be used in nonlinear-optical devices based on electromagnetically-induced transparency (EIT) [13, 14]. It is generally believed that the NV^- optical transitions between the ^3A ground states and ^3E excited states at zero magnetic field are almost perfectly spin-preserving [10]. This situation is advantageous for non-destructive readout of electron spins through fluorescence detection, but poses a problem for all-optical control of the electron spins. All-optical control requires a Λ system having two ground levels coupled to a common excited level. One solution is to work close to an avoided crossing of the $m_s = 0$ and $m_s = -1$ ground states that occurs at a particular magnetic field, as described in Ref. [15], where EIT was reported. However, previous spectral hole-burning studies [16, 17] suggest that the optical transitions are not always spin-preserving, even at zero magnetic field. In these experiments, anti-hole features (increases in fluorescence) were observed when two excitation lasers were separated by $\pm 2.88\,$GHz, the crystal-field splitting energy between the $m_s = 0$ and the degenerate $m_s = \pm 1$ ground states. These features can only appear if one or more excited states couples to both the $m_s = 0$ and $m_s = \pm 1$ levels. It is important therefore to establish better the conditions necessary for non-spin-preserving transitions for the design of devices based on EIT and all-optical control of electron spins.

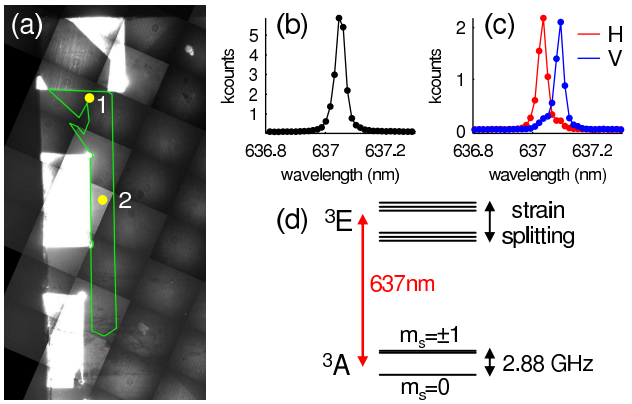

FIG. 1: (a) Large-scale photoluminescence (PL) image. The narrow-linewidth sector described in the text is outlined in green. (b) PL spectrum of the NV^- zero-phonon line measured at location 1 in the image. (c) Polarized PL spectra from location 2. "H" and "V" are for excitation and collection polarizations oriented horizontally and vertically, respectively, compared with the image. (d) Schematic energy level diagram for NV^-.

Here, we report spectral hole-burning experiments on a sample with little inhomogeneous broadening and a range of strain conditions obtained by ion implantation. We find that it is possible to realize a Λ system at zero magnetic field as confirmed through the observation of coherent population trapping [18, 19], the same mechanism involved in EIT. The results confirm that strain has a strong effect on the excited-state fine structure [17] and suggest that N-V centers can be engineered to have either spin-preserving or non-spin-preserving transitions as needed for a specific application.

The sample used for this study was a type 1b high-pressure, high-temperature (HPHT)-grown diamond crystal obtained originally from Sumitomo. Figure 1(a) shows a composite photoluminescence image obtained under 532 nm illumination. The bright squares were implanted with 2 MeV He at a fluence of $\sim 10^{16}$ cm^{-2}. The implantation breaks bonds, converting diamond to graphite. Expansion of the graphitized material produces tensile strain in the implanted region and compressive strain in the surrounding regions. Subsequent annealing at a temperature of 1400 °C for 15 minutes in vacuum combined vacancies with native nitrogen to create N-V centers. Although nitrogen occurs throughout the crystal, most of the luminescence was observed to originate from close to the surface. Another important feature of this sample is the presence of distinct sectors. Growth sectors are regions that have grown from particular faces of the original seed crystal. Because different

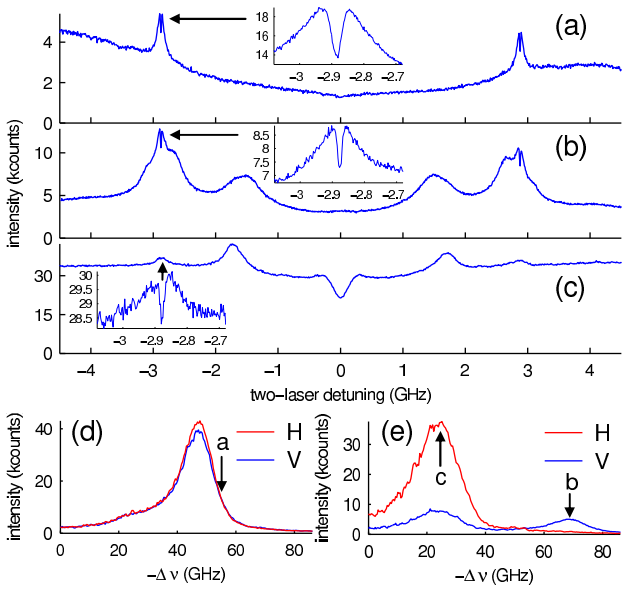

FIG. 2: (a,b,c) Two-laser scans showing anti-hole features and coherent population trapping effect at sample location 1 (a) and at location 2, measuring the long-wavelength (b) and short-wavelength (c) components of the zero-phonon line. Insets: higher-resolution scans of the −2.88 GHz features. Excitation powers: 5 μW for the 637 nm lasers and 2 μW for the repump. (d,e) Single-laser scans at locations 1 and 2, respectively. Arrows indicate spectral positions studied in (a,b,c).

faces grow at different rates and incorporate impurities at different levels, the sample shows marked discontinuities at sector boundaries. In two particular growth sectors, one of which is outlined in Fig. 1(a), the inhomogeneous linewidth of the NV^- zero-phonon line (ZPL) at 637 nm was approximately $10 - 20$ GHz, exceptionally narrow compared with the generally accepted value of 750 GHz [20]. Figs. 1(b,c) show low-temperature photoluminescence spectra from two locations, measured at 10 K using 532 nm excitation. At location 1 a single unpolarized peak was observed, while at location 2 the ZPL was split into two orthogonally polarized components. We attribute the splitting at location 2 to strain induced by the nearby implanted region, the edge of which is approximately parallel to one of the cubic crystal axes. By comparison with the stress measurements in Ref. [21], we estimate that the 44.5 GHz splitting corresponds to an equivalent uniaxial stress of 43 MPa. N-V centers can be oriented along four possible directions ([111], *etc.*), but the splitting should be the same in each case for strain along [100]. A schematic energy-level diagram, based on Refs. [22, 23], is shown in Fig. 1(d).

In the two-laser experiments, the zero-phonon line was excited on resonance using two

continuous-wave, tunable external-cavity diode lasers. One of the lasers (laser 2) was held fixed in frequency while the other (laser 1) was scanned over a range of up to 80 GHz. The scanning rate was calibrated by means of a Fabry-Perot cavity. The laser stability was approximately 1 MHz over short times and 10 MHz over a period of 10 minutes. A weak repump laser operating at 532 nm was also applied continuously to re-activate N-V centers that bleach after many fluorescence cycles, an effect that could be attributed to shelving [10] or photo-ionization [24]. The lasers were focused by a 0.6 numerical-aperture microscope objective through the cryostat window onto the sample surface with a spot size of approximately $3 - 4\,\mu$m. The resulting fluorescence was collected by the same objective, filtered to remove laser light, and sent to an avalanche-photodiode photon counter (Perkin-Elmer SPCM). A bandpass filter selected a 40 nm bandwidth centered at 700 nm for detection of emission into the broad phonon sidebands. This provided a measure of the N-V excited-state population. For most of the data shown below, laser 1 was scanned at a repetition rate of 1 Hz, and the results from many scans were summed.

Results from the two-laser measurements are shown in Fig. 2(a,b,c). These measurements were performed at the spectral locations indicated in the single-laser scans in Fig. 2(d,e), which show the overall shapes of the inhomogeneously broadened ZPLs. Each two-laser spectrum shows a pattern of peaks associated with the energy level structure and transition strengths at a particular location. As explained in Refs. [16, 17, 22], fluorescence peaks occur at two-laser detunings for which each laser is resonant with a transition in the same N-V centers involving different ground states. In these situations, the N-V center is excited from either ground state, producing constant fluorescence. If only one ground state is excited, the population is driven to the other ground state (optical pumping), and fluorescence is suppressed. Since the ground-state structure is relatively insensitive to strain [25], the variations between the two-laser spectra reflect differences in excited-state structure. The two-laser spectra are quite different between locations 1 and 2 and are also different for the two components of the strain-split ZPL at location 2. However, in all of the cases shown, peaks occur at detunings of $\pm 2.88 \pm 0.01$ GHz, matching the crystal-field splitting of the ground states. At these detunings the two lasers can couple two ground states to the same excited state.

The sharp dips appearing within the 2.88 GHz anti-holes are the signature of coherent population trapping. Close to two-photon resonance, a "dark state" can form, which is a

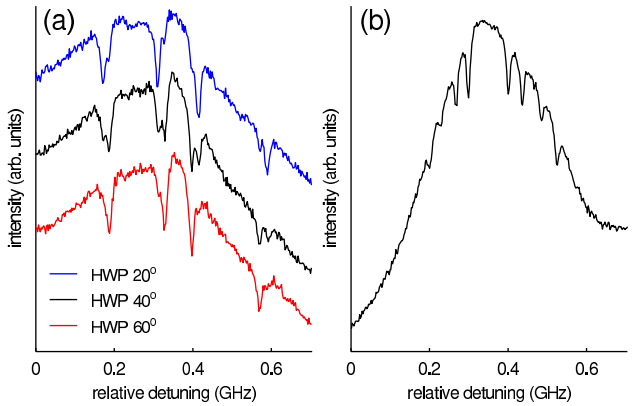

FIG. 3: Two-laser measurements with a weak magnetic field applied to lift the $m = \pm 1$ degeneracy. (a-c) Measured at location 1. HWP angles 20°, 40°, and 60° correspond to polarizations approximately along [110], [010], and [$\bar{1}$10], respectively. (d) Measured at location 2 for polarization along [010](V). All plots are scaled and shifted for clarity. The fluorescence decreases by approximately 8% for the dips in (a) and 4% for the dips in (b).

coherent superposition of ground states that has no net transition matrix element into an excited state due to destructive quantum interference [18, 19]. This feature only appears when the transition Rabi frequencies are large compared with the relevant decoherence rates. At location 1, where no strain splitting is resolved, the effect was only observed on the long-wavelength side of the ZPL. On the short wavelength side, the anti-hole pattern was different, and the 2.88 GHz anti-holes were almost absent. The random fluctuations in strain or electric field responsible for the inhomogeneous broadening apparently has a strong effect on the excited-state fine structure and optical transitions [17]. The only distinct anti-hole at this location is the 2.88 GHz feature associated with the ground-state splitting, suggesting a random variation in the excited-state structure. However, at location 2, where strain splitting is resolved, we observed distinct anti-holes associated with the excited-state structure. Coherent population trapping was more easily observed in the long-wavelength component of the strain-split doublet, where the 2.88 GHz anti-holes are prominent. In the short-wavelength component, the excited-state structure is different, and the 2.88 GHz anti-holes are much smaller, suggesting optical transitions that are more nearly spin-preserving. It is clear from these measurements and from measurements we have performed elsewhere on this sample that small amounts of strain cause large changes in the excited-state fine structure.

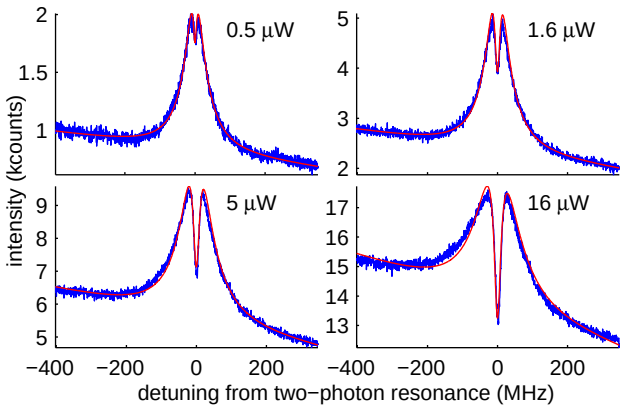

FIG. 4: Coherent population trapping at various excitation powers at location 1 (same as in Fig. 2a). The indicated powers correspond to both 637 nm lasers. Fitted Rabi frequencies, same for both transitions (a-d): 7.2, 12.7, 17.6, and 21.6 MHz; effective population decay rates between ground states (a-d): 0.07, 0.17, 0.34, and 0.83 MHz; excited-state decoherence: 4.3, 2.4, 4.1, and 7.7 MHz. blue:data, red:fits.

At zero magnetic field it is possible for all four orientations of N-V centers to show coherent population trapping behavior. To determine the orientation dependence, we performed two-laser measurements with a weak magnetic field (~ 100 Gauss) applied to lift the degeneracy of the $m_s = \pm 1$ ground states. The magnetic field direction was adjusted so that each of the four orientations had a different energy splitting. As shown in Fig. 3, the fluorescence dip on two-photon resonance splits into a maximum of eight components corresponding to the four orientations. For the unstrained region (location 1), the fluorescence dips are divided into two groups responding to polarizations along [110] and $[1\bar{1}0]$. We expect that one polarization primarily excites N-V centers oriented along [111] and $[\bar{1}\bar{1}1]$, while the other polarization primarily excites centers oriented along $[1\bar{1}\bar{1}]$ and $[\bar{1}1\bar{1}]$. For polarization along [010], all four orientations produce fluorescence dips. For the long-wavelength peak at location 2, eight fluorescence dips appear for [010] polarization, showing that all four orientations can participate even in the strained case. The possibility of obtaining equivalent Λ systems for all four orientations is an advantage over the anti-crossing scheme in Ref. [15], where only one orientation participated.

Finally, we show that the shape and excitation power dependence of the 2.88 GHz peaks can be explained by a theoretical model that takes into account the inhomogeneous broaden-

ing of the ground-to-excited-state transitions. The power dependence measured at location 1 is shown in Fig. 4. At low power, a shallow dip approximately 10 MHz wide appears which then deepens and broadens with increasing power. To fit these data, we use a simplified model with three levels in a Λ configuration. The two ground states represent the $m = 0$ ($|1\rangle$) and $m = \pm 1$ ($|2\rangle$) levels of the ground state manifold, with a fixed frequency difference of 2.88 GHz. The excited state ($|3\rangle$) is given a variable frequency following a normal (gaussian) distribution ($\sigma = 10$ GHz). The model includes all possible population relaxation and dephasing terms under the simplifying assumption that the relaxation rates and transition strengths are the same for the two lower levels. We first find the steady-state density matrix for a single center and then average over the inhomogeneous distribution. The fitted curves, shown in Fig. 4, are proportional to the steady-state population of the excited state, plus a linearly sloped background added as an additional fitting parameter representing contributions from other subsets of levels. The theoretical curves match the data quite well, confirming that the observed behavior can be explained in terms of an inhomogeneous distribution of three-level systems. From the fits we estimate that the pure dephasing rate between the excited and ground states is $\gamma_{13} \sim 4$MHz, which should be compared with the radiative linewidth of 13.4 MHz used in the fits. The fits unambiguously determine the value of the important decoherence parameter γ_{12} between the two ground states, since this parameter is closely related to the shape of the dip within the anti-hole feature. We find $\gamma_{12} = 3.8 \pm 1$ MHz. Laser instability can contribute to the decoherence, but preliminary measurements using an electro-optic modulator in place of a second laser suggest that the true γ_{12} is not much smaller for this sample. Possible sources of ground-state broadening include inhomogeneous variation of the ground-state crystal-field splitting [25], stray magnetic fields affecting the four orientations differently, interactions with N impurities [6] and hyperfine coupling with ^{14}N and ^{13}C nuclei. The much longer coherence lifetime of 58 μs reported in Ref. [2] was obtained using spin-echo techniques to remove the effect of inhomogeneous broadening.

The coherent population trapping effects reported here suggest that EIT and all-optical spin manipulation should be possible with N-V centers even at zero magnetic field. A small amount of strain, which can be introduced through ion implantation or other fabrication methods [26], is sufficient for choosing between spin-preserving and non-spin-preserving optical transitions. For certain directions of strain, all four orientations can produce a similar

Λ system. We conclude that N-V centers have a flexibility in their excited-state level structure that makes them suitable either for single-spin readout through fluorescence detection or for optical devices based on EIT and Raman transitions.

We thank S. Shahriar and P. Hemmer for helpful discussions. The work performed at HP Laboratories in Palo Alto has been supported in part by DARPA contract no. FA9550-05-C-0017. Quantum Communications Victoria is supported by the State Government of Victoria's Science, Technology and Innovation Initiative - Infrastructure Grants Program. BCG is proudly supported by the *International Science Linkages* programme established under the Australian Government's innovation statement *Backing Australia's Ability*. This work was supported by the DEST, Australian Research Council, the Australian government and by the US National Security Agency (NSA), Advanced Research and Development Activity (ARDA) and the Army Research Office (ARO) under contracts W911NF-04-1-0290 and W911NF-05-1-0284.

---

* Electronic address: `charles.santori@hp.com`

[1] B. E. Kane, Nature (London) **393**, 133 (1998).

[2] T. A. Kennedy, J. S. Colton, J. E. Butler, R. C. Linares and P. J. Doering, Appl. Phys. Lett. **83**, 4190 (2003).

[3] F. Jelezko *et al.*, Appl. Phys. Lett. **81**, 2160 (2002).

[4] E. A. Wilson, N. B. Manson, and C. Wei, Phys. Rev. A **67**, 023812-1 (2003).

[5] F. Jelezko, T. Gaebel, I. Popa, M. Domhan, A. Gruber, and J.Wrachtrup, Phys. Rev. Lett. **93**, 130501 (2004).

[6] R. J. Epstein, F. M. Mendoza, Y. K. Kato, and D. D. Awschalom, Nature Physics **1**, 94 (2005).

[7] C. Kurtsiefer, S. Mayer, P. Zarda, and H. Weinfurter, Phys. Rev. Lett. **85**, 290 (2000).

[8] A. Beveratos, S. Kühn, R. Brouri, T. Gacoin, J.-P. Poizat, and P. Grangier, Eur. Phys. J. D **18**, 191 (2002).

[9] L. Childress, J. M. Taylor, A. S. Sorensen, and M. D. Lukin, Phys. Rev. A **72**, 052330-1 (2005).

[10] A. P. Nizovtsev *et al.*, Opt. Spectrosc. **99**, 233 (2005).

[11] A. D. Greentree *et al.*, preprint.

[12] M. S. Shahriar, P. R. Hemmer, S. Lloyd, P. S. Bhatia, and A. E. Craig, Phys. Rev. A **66**, 032301 (2002).

[13] H. Schmidt and A. Imamoglu, Opt. Lett. **21**, 1936 (1996).

[14] W. J. Munro, K. Nemoto, R. G. Beausoleil, and T. P. Spiller, Phys. Rev. A **71**, 033819 (2005).

[15] P. R. Hemmer, A. V. Turukhin, M. S. Shahriar, and J. A. Musser, Opt. Lett. **26**, 361 (2001).

[16] N. R. S. Reddy, N. B. Manson, and E. R. Krausz, J. Lumin. **38**, 46 (1987).

[17] N. B. Manson and C. Wei, J. Lumin. **58**, 158 (1994).

[18] G. Alzetta, A. Gozzini, L. Moi, and G. Orriols, Nuovo Cimento **36B**, 5 (1976).

[19] H. Gray, R. Whitley, and J. C. R. Stroud, Opt. Lett. 3, 218 (1978).

[20] A. M. Zaitsev, *Optical Properties of Diamond: A Data Handbook* (Berlin: Springer, 2001).

[21] G. Davies and M. F. Hamer, Proc. R. Soc. London Ser. A **348**, 285 (1976).

[22] J. P. D. Martin, J. Lumin. **81**, 237 (1999).

[23] N. B. Manson, J. P. Harrison, and M.J. Sellars, *preprint*: arXiv:cond-mat/0601360

[24] N. B. Manson and J. P. Harrison, Diamond & Related Materials **14**, 1705 (2005).

[25] E. van Oort, B. van der Kamp, R. Sitters, and M. Glasbeek, J. Lumin. **48 & 49**, 803 (1991).

[26] P. Olivero *et al.*, Advanced Materials **17**, 2427 (2005).